Article:

Huang, X., Yang, S., Haywood, A. et al. (2026) Weakened El Niño/La Niña Influence on the East Asian Summer Monsoon Under Pliocene Warmth: Insights From Model Sensitivity Experiments. Journal of Geophysical Research: Atmospheres, 131 (12). e2026JD046302. ISSN: 2169-897X

https://doi.org/10.1029/2026jd046302

Weakened El Niño/La Niña influence on the East Asian summer monsoon under Pliocene warmth: Insights from model sensitivity experiments

Xiaofang Huang[1], Shiling Yang[1,2*], Alan Haywood[3], Julia Tindall[3], Minmin Sun[1], Xiaoxiao Yang[4], Hongmei Li[1], Wenying Jiang[1]

[1]State Key Laboratory of Lithospheric and Environmental Coevolution, Institute of Geology and Geophysics, Chinese Academy of Sciences, Beijing 100029, China, [2]College of Earth and Planetary Sciences, University of Chinese Academy of Sciences, Beijing 100049, China, [3]University of Leeds, Leeds, LS2 9JT, UK, [4]Institute of Geomechanics, Chinese Academy of Geological Sciences, Beijing, China

*Corresponding author.

Email: yangsl@mail.iggcas.ac.cn (S. Yang)

Key points:

- East Asian summer monsoon precipitation consistently increases under both El Niño– and La Niña–like conditions during Pliocene warmth
- The modern El Niño/La Niña–related dipole/tripole precipitation pattern shifts to a monopole-like increase in Pliocene East Asian rainfall
- Increased atmospheric moisture under a Pliocene-like warm climate leads to a weakened El Niño/La Niña–monsoon relationship

Abstract: The impact of the El Niño–Southern Oscillation (ENSO) on East Asian summer monsoon (EASM) precipitation under sustained warming remains uncertain. Through Pliocene-like simulations, we demonstrate that under a permanent El Niño–like phase, an eastward-shifted Walker Circulation triggered a low-level anticyclone over the South China Sea and prompted a southward shift of the westerly jet via a Rossby wave train. This circulation configuration facilitated the influx of abundant moisture into East Asia, consequently enhancing regional precipitation, particularly in southern China. In contrast, under a permanent La Niña–like phase, a westward-intensified Walker Circulation generated a low-level cyclone over the East China Sea and a coastal anticyclone, strengthening moisture transport into East Asia, with the most pronounced increases in precipitation occurring in central-eastern China. We attribute the consistent wetting trends in East Asia across both ENSO phases to the increased moisture-holding capacity of a warmer atmosphere, which enhances rainfall efficiency irrespective of differing circulation patterns. Our findings indicate a paradigm shift in the El Niño/La Niña–monsoon relationship, transitioning from the contemporary dipole/tripole precipitation response to a regime in which both ENSO phases result in a broad, monopole-like increase in East Asian rainfall in a warming climate. This suggests a weakened El Niño/La Niña influence on the East Asian summer monsoon precipitation under Pliocene-like warming conditions. These evolving El Niño/La Niña–monsoon dynamics must be considered when interpreting proxy records from past warm periods and projecting future climate impacts.

Plain Language

ENSO strongly influence summer rainfall in East Asia today, but it remains unclear how this relationship may change in a much warmer climate. To address this question, we used climate simulations representing Pliocene-like warming, a period in Earth's past that was warmer than today. We examined two idealized scenarios: one with persistent El Niño–like conditions and one with persistent La Niña–like conditions. In the El Niño–like climate, the Pacific Walker Circulation shifted eastward, altering large-scale atmospheric flow and enhancing moisture transport into East Asia, leading to increased summer rainfall, especially in southern China. In the La Niña–like climate, the Walker Circulation intensified westward, producing a different circulation pattern that also increased moisture transport, with the largest rainfall increases in central-eastern China. Despite these different circulation responses, East Asia became wetter in both cases. This occurs because a warmer atmosphere can hold more water vapor, making rainfall more efficient regardless of ENSO phase. Our results suggest that under sustained warming, the modern El Niño/La Niña–related contrast in East Asian summer rainfall may weaken, with both El Niño and La Niña leading to broadly increased rainfall. This has important implications for interpreting past warm climates and projecting future regional climate change.

Introduction

The East Asian summer monsoon (EASM) is a critical climate system that governs weather patterns across densely populated East Asia. As a key component of global atmospheric circulation, it facilitates critical heat and moisture exchange between the Northern and Southern Hemispheres (Ding, 2004; Webster et al., 1998). Monsoon rainfall supports more than half the world's population (Liu, 1999), yet its variability—manifested by extreme floods and droughts—often leads to significant human casualties and socioeconomic disruptions (Xie et al., 2016; Yu et al., 2025).

The predictability of the EASM in the near future can be modulated by several factors (e.g., El Niño–Southern Oscillation (ENSO), Pacific Decadal Oscillation, Indian Ocean Dipole, Atlantic Multidecadal Oscillation), among which the ENSO has been identified as the most critical one (Hu et al., 2017; Wang et al., 2000; Yang et al., 2022; Zhang et al., 2024). Numerous studies have revealed highly complex relationships between ENSO and the EASM, which can be summarized by the following four aspects. First, El Niño events generally induce a "southern flood–northern drought" pattern in China, whereas La Niña events are typically associated with the opposite "southern drought–northern flood" regime (Chen et al., 1991; Gao et al., 2014). Some studies, however, even suggest a tripole precipitation pattern over mainland China induced by ENSO events (Huang and Hu, 1989; Liu et al. 2008; Sun et al. 2021; Li et al., 2026). Second, the frequency of ENSO events has increased with global warming (Trenberth et al., 2002; Wu et al., 2001; Xia et al., 2017), with increased ENSO frequency leading to a weakened EASM (Liu et al., 2000; Long and Li, 2001; Zhu et al., 1999). Third, the relationship between ENSO and the EASM is unstable over long timescales (Jiang et al., 2003; Song and Zhou, 2015; Wang and Fan, 2013; Luo et al., 2025), showing periodic characteristics (Jiang et al., 2003; Song and Zhou, 2015; Wang and Fan, 2013):

significant negative correlations between monsoon precipitation and ENSO occurred during 1892–1912 and 1979–1999, while weak relationships occurred during 1914–1934 and 1958–1978. Fourth, the influence of ENSO on the EASM has weakened under global warming since the 2000s (Yu et al., 2025).

The atmospheric CO_2 concentration currently exceeds 400 ppmv. However, due to the substantial thermal inertia of the oceans, the ocean–atmosphere system has not yet reached equilibrium in response to current warming (Back et al., 2013; Levitus et al., 2000), making it challenging to assess the effect of ENSO on the EASM under global warming. The discrepancy in proposed ENSO–EASM relationships stems from a lack of understanding of ENSO's sensitivity to climate variability under equilibrated conditions (White and Ravelo, 2020). Clearly, investigating the influence of El Niño/La Niña on the EASM during past natural warm periods provides a key framework for projecting future climate change.

Palaeoclimate studies have indicated that the Late Pliocene Warm Period (LPWP; 3.264–3.025 Ma) is a valuable analogue for end-of-century climate conditions (Burke et al., 2018; Haywood et al., 2016; McClymont et al., 2020). This is because: 1) it is the most recent geological epoch with atmospheric CO_2 concentrations exceeding 400 ppmv (Huang et al., 2019, 2021); 2) continental configurations during the LPWP were similar to those of today (Huang et al., 2019, 2021); and 3) global mean temperatures during the LPWP were ~2–3°C higher than pre-industrial levels (Haywood et al., 2013), closely resembling the climate projections for the late 21st century under high-emission scenarios (IPCC, 2013). Therefore, the LPWP is well suited for studying the influence of El Niño/La Niña on the EASM under equilibrated high-CO_2 conditions.

Geological evidence suggests that the ENSO may have originated as early as the Mesozoic and remained active through the Cenozoic (Cane 2005; Galeotti et al. 2010; Ivany et al. 2011; Li et al., 2024; Manucharyan and Fedorov, 2014; Watanabe et al., 2011), indicating that ENSO variability may have long been a prominent feature of Earth's climate system (Cai et al., 2021). Nonetheless, paleo-proxies for ENSO activity during the LPWP are very limited and have large uncertainties (Fedorov and Philander, 2001; Fedorov et al., 2006; Ravelo et al., 2004; Rickaby et al., 2005; Wara et al., 2005;

Watanabe et al., 2011; Winnick et al., 2013; Wycech et al., 2020), hindering our understanding of the El Niño/La Niña–EASM relationship. Numerical simulations are a valuable tool for exploring past climates on both regional and global scales, providing key insights into the impact of El Niño/La Niña on the EASM under equilibrated climate conditions. Here, we performed sensitivity experiments using a coupled climate model to explore the ENSO–EASM relationship during the Pliocene, and its mechanism, to provide an improved perspective on future climate change.

2 Methods

2.1 Model description

The Hadley Centre Coupled Model, version 3 (HadCM3), is a widely used general circulation model (GCM) developed by the UK Met Office Hadley Centre. It couples atmosphere (2.5° × 3.75°, 19 levels) and ocean (1.25° × 1.25°, 20 levels) components without requiring flux adjustments (Gordon et al., 2000; Pope et al., 2000; Valdes et al., 2017), making it stable for long-term climate simulations. The atmospheric model has a time step of 30 min and includes a radiation scheme that can represent the effects of major and minor trace gases (Edwards and Slingo, 1996). The ocean model is a ‘rigid lid’ model, with a time step of one hour and incorporates a thermodynamic–dynamic sea ice model with primitive (ocean drift) dynamics. HadCM3 has been key in IPCC assessments, paleoclimate studies, and future climate projections, known for its computational efficiency and reliability in large-scale simulations. This model has been used extensively for studies of the Pliocene within the Pliocene Model Intercomparison Project experiments (Bragg et al., 2012; Haywood et al., 2010, 2011; Hunter et al., 2019).

2.2 Pliocene boundary conditions and experimental designs

Modeling efforts focused on the LPWP, known as the Pliocene Model Intercomparison Project (PlioMIP), utilized PRISM (Pliocene Research, Interpretation and Synoptic Mapping) reconstructions. For this study, the required late Pliocene boundary conditions were supplied by the PRISM dataset, specifically the latest iteration of the reconstruction known as PRISM4 (Dowsett et al., 2016; Table S1). They include topography and bathymetry, coastlines, land surface properties (i.e., vegetation, soil type, and ice sheet cover) and atmospheric composition with respect to pre-industrial conditions.

To evaluate the effect of El Niño/La Niña on the EASM, three modelling experiments are presented here: one late Pliocene control run (hereafter LPControl), one representing permanent El Niño–like conditions and one representing permanent La Niña–like conditions. The control simulation was started from the end of the HadCM3 contribution to the PlioMIP2 simulation (Hunter et al., 2019). There was a difference between our control simulation and the PlioMIP2 simulation, namely we used dynamic vegetation, while Hunter et al. (2019) used fixed vegetation from PRISM4. The permanent El Niño–like and La Niña–like experiments were set up following Haywood et al. (2007), as follows:

Firstly, sea surface temperature reference files were created to represent permanent El Niño– and La Niña–like conditions. During model integration, a Haney restoring term was applied at each timestep to relax the simulated SST toward these reference fields, according to the following equation:

$$Anom\_heat = \alpha * (Tref - T)$$

Where T is the temperature from the simulation, Tref is the temperature in the sea surface temperature reference files, and α depends on location. In our case, α was set to 170W m^{-2} K^{-1} (to represent a 14-day timescale) over the 40°N–40°s, and zero everywhere else. In both experiments, only the SST over the entire Pacific was relaxed (Figure S1).

For the El Niño experiment, SST across the tropical Pacific was restored toward the mean temperature of the western Pacific warm pool, effectively eliminating the east–west SST gradient and creating a basin-wide warming pattern. For the La Niña experiment, the reference SST field was constructed by amplifying the zonal contrast. The average temperature across the Pacific was calculated, and then the SST at each grid point was adjusted as:

T_new(x, y) = T_avg + 1.5 × (T_ref(x, y) – T_avg)

to make the Pacific warm gridboxes on a latitudinal circle slightly warmer and the cold gridboxes slightly colder.

All experiments are initialized from the end of the HadCM3 PlioMIP2 simulation and are integrated for an additional 100 model years to achieve equilibrium with the prescribed boundary conditions. Climate statistics are derived from the final 30 years of each run. Results are presented as anomalies from the control experiment to isolate the effect of El Niño/La Niña on the EASM during the LPWP.

2.3 Definitions of climate indices

To investigate the mechanisms by which ENSO influenced East Asian summer monsoons during the LPWP, we analyzed variations in El Niño/La Niña–related subtropical highs, moisture fluxes, Rossby waves, and Walker circulation. Specifically, changes in monsoonal circulation were characterized as follows: wind field anomalies at 850 hPa and 500 hPa; shifts in moisture sources were demonstrated through vertically integrated water vapor transport; the position of the western Pacific subtropic high is conventionally measured by the 0-gpm contour lines of the 850-hPa eddy geopotential height (i.e. the anomaly between the 850-hPa geopotential height and the zonal mean of the 850-hPa geopotential height (Huang et al., 2015); and the zonal mass streamfunction Ψ, which intuitively depicts the tropical Pacific Walker circulation (PWC) structure characterized by an enclosed and clockwise rotation cell in the zonal–vertical section over the equatorial Pacific (Yu and Zwiers, 2010; Yu et al., 2012), was used to study the changes in PWC spatial structure during the LPWP.

3 Monsoon precipitation changes

The simulated precipitation changes over the East Asian monsoon region during summer (June–August) were analyzed (Figure 1). The anomalies between the El Niño experiment and the late Pliocene control experiment (Figure 1a, b) revealed a general increase in precipitation over China, with the most pronounced enhancement in southern China (>2 mm day^{-1}) and a moderate rise in northern regions (~0.5–1.5 mm day^{-1}). In contrast, relative to the late Pliocene control experiment, the La Niña experiment exhibited increased precipitation over most of China, with the largest increases occurring in central and eastern China, while only limited regions in the southwest experienced reduced precipitation (Figure 1c). Clearly, contrary to the traditional ENSO dipole/tripole precipitation response (Gao et al., 2014; Sun et al. 2010; Li et al., 2026), warm-climate responses exhibited a monopole-like increase in East Asia (Figure 1). The annual mean precipitation anomalies show a similar spatial pattern (Figure S2).

Consistent with the precipitation response, summer mean relative humidity over East Asia also exhibited a coherent increase under both ENSO phases (Figure 1d–f). In the late Pliocene control experiment, relative humidity displays a climatological pattern characterized by higher values over southern and eastern China and lower values over inland regions (Figure 1d). Relative to the control experiment, the El Niño experiment showed a widespread increase in relative humidity across East Asia (Figure 1e), with the largest enhancements occurring over North China (~10–15%), and a more moderate increase over southern China (0–10%). Similarly, in the La Niña experiment, relative humidity increased over most of East Asia compared to the control (Figure 1f), with maximum increases also centered over North China (up to 15%). Overall, the relative humidity anomalies further confirmed that enhanced atmospheric moisture availability under Pliocene-like warming contributes to the widespread intensification of summer rainfall across East Asia.

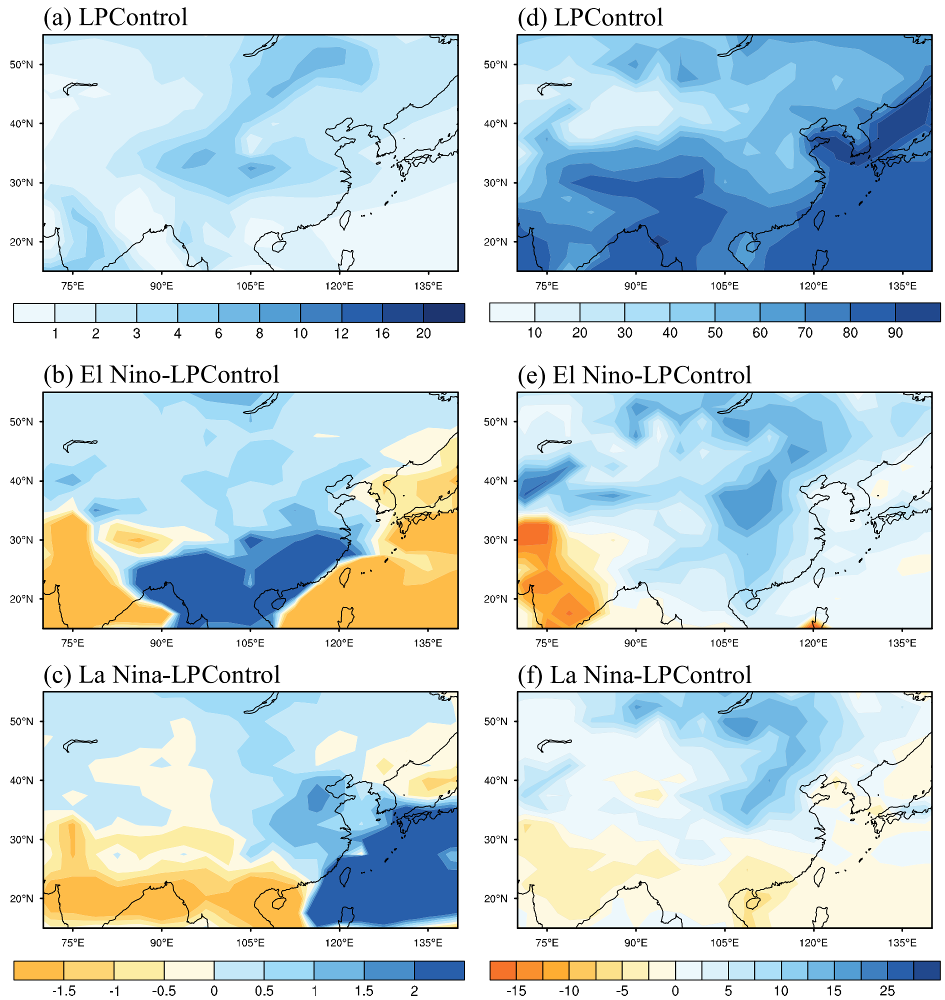

Figure 1. Summer mean precipitation and relative humidity distribution and anomalies. (a) Summer mean precipitation in the late Pliocene control experiment (LPControl; units: mm day^{-1}); (b) Summer mean precipitation anomalies (units: mm day^{-1}) between the El Niño experiment and the late Pliocene control experiment; (c) Summer mean precipitation anomalies (units: mm day^{-1}) between the La Niña experiment and the late Pliocene control experiment. The right panels show the corresponding distribution and anomalies of relative humidity. Summer spans June–August (JJA).

4 Mechanisms

4.1 Upper-/lower-level circulation adjustments and moisture supply

The 850 hPa wind and vertically integrated moisture flux anomalies revealed distinctly organized dipole structures that modulated the transport of moisture into East

Asia under both ENSO phases. In the El Niño experiment, an anomalous anticyclone centered over the South China Sea (10–30°N, 110–130°E; Figure 2a, b) enhanced southwesterly moisture transport along its northwestern periphery (Figure 3b), while a coexisting cyclonic anomaly over the northwest Pacific (20–50°N, 140–180°E; Figure 2b) reinforced convergent flow over northeastern Asia (10–30°N, 130–140°E; Figure 2b). Conversely, during La Niña–like conditions, a cyclonic anomaly over the East China Sea (20–40°N, 110–140°E; Figure 2c) transported moisture toward the Yangtze Basin (Figure 3c), amplified by an adjacent western Pacific anticyclone (Figure 2c).

Critically, both configurations enhanced moisture convergence over continental East Asia despite opposite rotational dynamics: El Niño's anticyclone-southwesterly conveyor favored the Chinese Mainland, especially southern China, whereas La Niña's cyclone-driven southeasterly flow targeted central-eastern China. This suggests that the warming-induced increase in atmospheric moisture—by ~7% per degree Celsius, as governed by the Clausius–Clapeyron relationship (Trenberth et al., 2005)—transforms the traditionally ENSO-induced dipole/tripole precipitation response into a monopole-like increase in monsoon rainfall, even though the spatial distribution of monsoon precipitation remains modulated by circulation changes. This interpretation is strongly supported by the column-integrated moisture content changes (Figure 3e, f), which show that under both ENSO phases, moisture content increases substantially not only across East Asia but also over the extremely dry interior of Asia.

To resolve the dynamical drivers of these moisture pathways—particularly the role of subtropical steering flows—we examined mid-tropospheric circulation adjustments, including 500 hPa wind anomalies (Figure 2d–f) and the western Pacific subtropical high (WPSH) position (Figure 4).

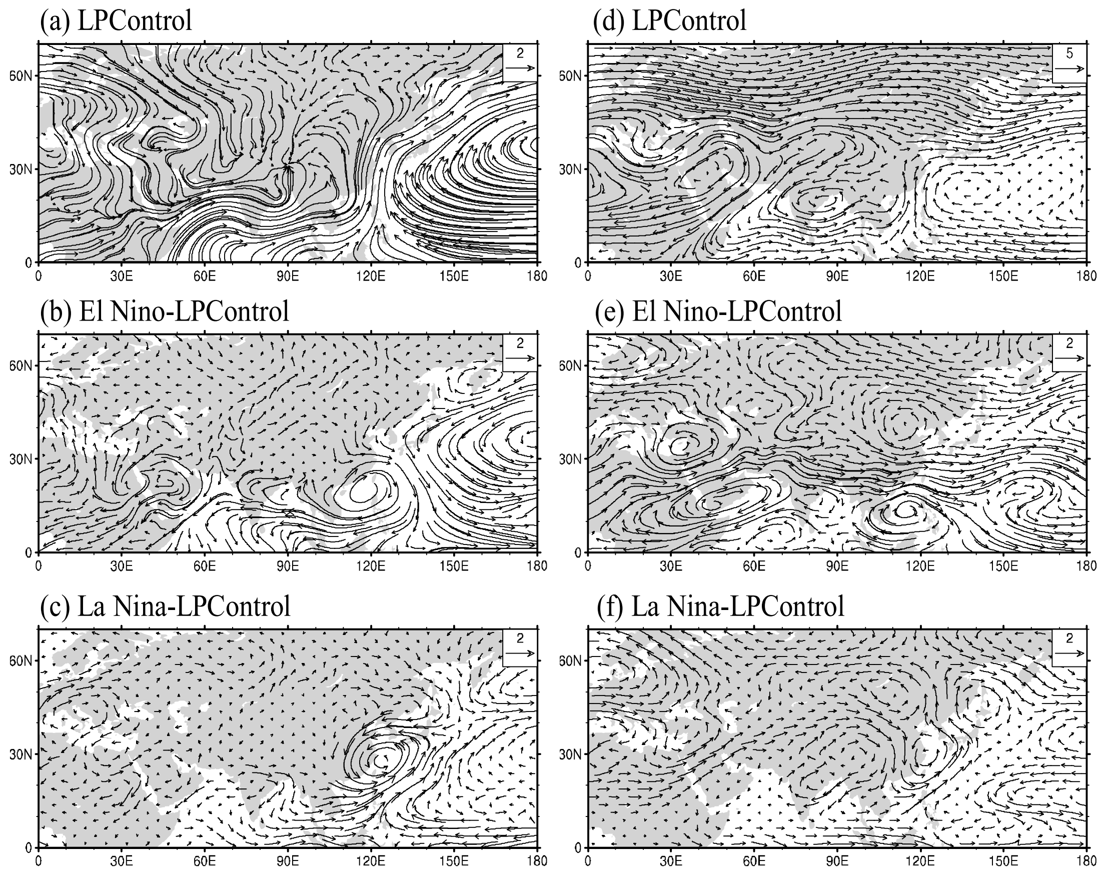

Figure 2. Summer mean 850 hPa (left panel) and 500 hPa (right panel) wind field distribution and anomalies. (a) Summer mean 850 hPa wind field distribution for the late Pliocene control experiment (LPControl; units: m s^{-1}); (b) Summer mean 850 hPa wind field anomalies (units: m s^{-1}) between the El Niño experiment and the late Pliocene control experiment; (c) Summer mean 850 hPa wind field anomalies (units: m s^{-1}) between the La Niña experiment and the late Pliocene control experiment. The right panels are the same as the left panels but for the 500 hPa level. Summer spans June–August (JJA)

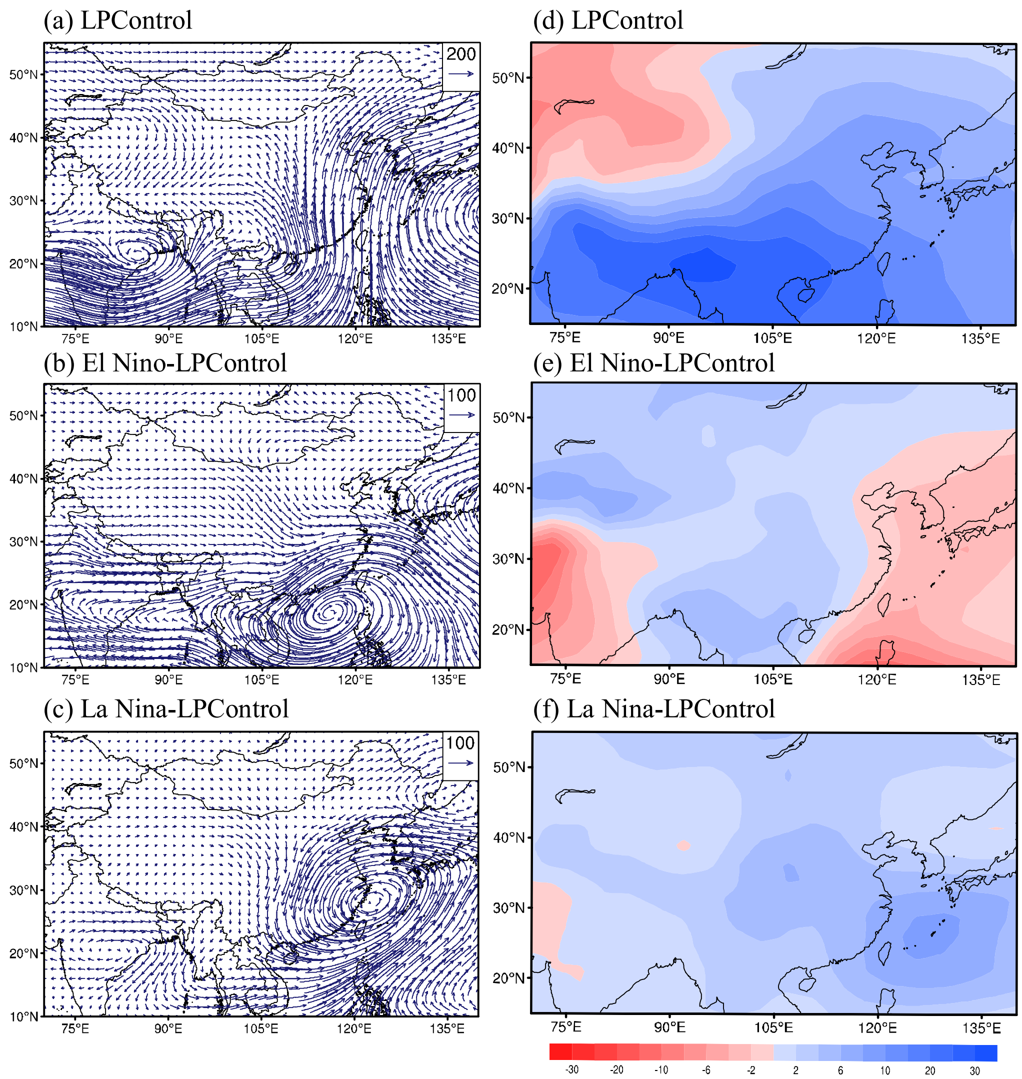

Figure 3. Summer mean vertically integrated water vapor flux (units: kg m^{-1} s^{-1}) and the column-integrated atmospheric moisture content (units: kg m^{-2}) distribution and anomalies. (a) Summer mean vertically integrated water vapor flux distribution for the late Pliocene control experiment (LPControl; arrows, units: kg m^{-1} s^{-1}); (b) Summer mean vertically integrated water vapor flux anomalies (arrows, units: kg m^{-1} s^{-1}) between the El Niño experiment and the late Pliocene control experiment; (c) Summer mean vertically integrated water vapor flux anomalies (arrows, units: kg m^{-1} s^{-1}) between the La Niña experiment and the late Pliocene control experiment. The right panels are the same as the left panels but for the column-integrated atmospheric moisture content (units: kg m^{-2}). Summer spans June–August (JJA).

Mid-tropospheric circulation adjustments revealed fundamental controls on the lower-level moisture pathways identified earlier. Under El Niño–like forcing, a baroclinic structure emerged: while the 850 hPa layer exhibited a South China Sea anticyclone (enhancing low-level southwesterlies; Figure 2b), the 500 hPa level featured a cyclonic anomaly over northern China (115–125°E, 35–45°N; Figure 2e) and an anticyclonic response over the South China Sea (Figure 2e). This vertical tilt corresponded to the intensification and northwestward extension of the western Pacific subtropical high (WPSH; Figure 4). This configuration had two effects: (i) it steered moist southwesterly winds from the low-level anticyclone toward Chinese Mainland; and (ii) it triggered mid-tropospheric ascent over North China via cyclonic vorticity advection, thereby enhancing monsoon precipitation.

Conversely, La Niña–like conditions generated a 500 hPa dipole (Figure 2f)—an anticyclone over northeast Asia (40–55°N, 135–150°E) and a cyclone over the coastal eastern China (25–35°N, 110–130°E)—coincident with eastward WPSH retreat (Figure 4). This configuration anchored the low-level cyclonic anomaly (20–40°N, 110–140°E) observed at 850 hPa, enhancing its easterly moisture transport into central-eastern China.

Critically, WPSH repositioning in both phases redirected moist airflow from lower levels: westward/northward expansion during the El Niño experiment transported moisture towards the Chinese Mainland, whereas La Niña's eastward contraction concentrated convergence over central-eastern China. This explained the spatial difference in precipitation anomalies—characterized by maximum increases over southern China during El Niño–like conditions and over central-eastern China during La Niña–like conditions—despite consistent wetting over East Asia, with the warm background ensuring abundant moisture supply to support ascent under either dynamical regime.

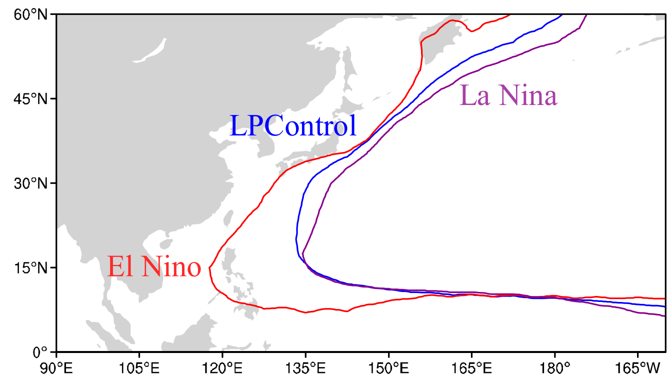

Figure 4. Zero contour lines of the 850-hPa eddy geopotential height field for (a) the El Niño experiment (red), (b) the La Niña experiment (purple), and (c) the late Pliocene control experiment (LPControl; blue).

4.2 ENSO modulation of the westerly jet

The 500 hPa geopotential height (Z500) anomalies exhibited hemispheric-scale Rossby wave responses to El Niño/La Niña forcing, with critical differences in latitudinal positioning and longitudinal nodes (Figure 5). Under El Niño–like conditions, a pronounced wave train emerged between 30°N and 60°N, featuring negative anomalies centered near 30°E (North Atlantic), 80°E (Central Asia), and 140°E (Northwest Pacific), interspersed with positive lobes (Figure 5b). Crucially, the wave train directly shaped the regional circulation. The trough near 140°E anchored the mid-level cyclonic anomaly over northern China (115–125°E, 35–45°N; Figure 2e), while the relatively higher geopotential height over East Asia (110–130°E) reinforced the pressure gradient, supporting the northwestward extension of the WPSH (Figure 4). This specific wave pattern enhanced baroclinicity along the northern flank of the WPSH, promoting ascent in the convergence zone where the low-level southwesterly flow (from the South China Sea anticyclone) met the mid-latitude westerlies.

Conversely, La Niña caused a poleward shift of the wave train (40–70°N) with troughs at 65°E (Caspian Sea) and 180°E (International Date Line) (Figure 5c). The trough at 180°E played a decisive role in shaping the East Asian climate by triggering a quasi-stationary wave pattern that extended its influence southwestward toward the East Asian coast: (i) It generated a high-pressure anomaly (a ridge) off the East Asian coast (120–140°E). This downstream ridge is the direct cause of the observed 500 hPa anticyclone over northern China (Figure 2f). The presence of this strong anticyclonic anomaly over the coastal region effectively pushed the WPSH eastward (Figure 4). (ii) This new pressure pattern—a trough at 180°E followed by a ridge near the coast—accelerated the westerly jet. The intensified westerlies then captured and steered the moist southeasterly flow along the eastern flank of the low-level cyclone (110–140°E; Figure 2f), channeling moisture into the Yangtze Basin and enhancing precipitation there.

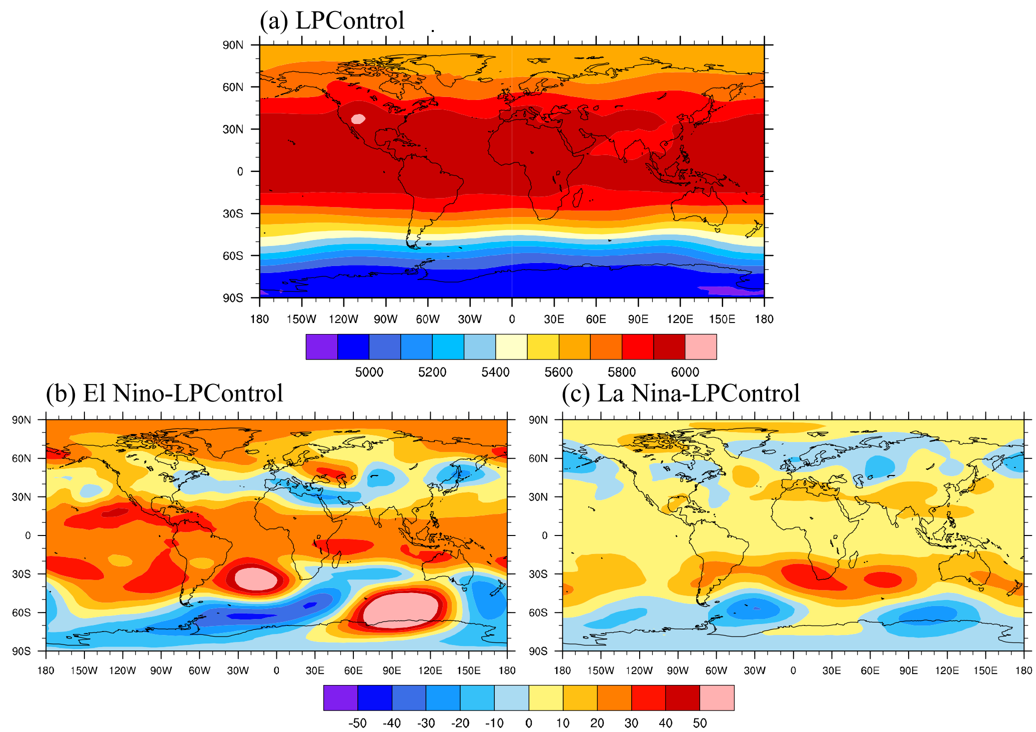

Figure 5. Summer mean 500 hPa geopotential height field distribution and anomalies (units: m). (a) Summer mean 500 hPa geopotential height field (units: m) for the late Pliocene control experiment (LPControl; units: m); (b) Summer mean 500 hPa geopotential height field anomalies between the El Niño experiment and the late Pliocene control experiment (units: m); and (c) Summer mean 500 hPa geopotential height field anomalies between the La Niña experiment and the late Pliocene control experiment. Summer spans June–August (JJA).

4.3 Changes in the tropical Pacific Walker Circulation

The zonal mass streamfunction (Ψ) anomalies revealed a fundamental reorganization of the tropical Pacific Walker Circulation (PWC; Figure 6), elucidating the tropical forcing behind the extratropical wave trains and moisture steering documented earlier. For the El Niño experiment, Ψ decreased by > 10 units over 130°E–150°W, indicating a weakened ascending branch over the Maritime Continent (Figure 6b). Concurrently, Ψ intensified by > 10 units east of 150°W (90°W–150°W; Figure 6b), signaling enhanced ascent over the central-eastern Pacific. The dipole pattern of negative Ψ anomalies over the western Pacific and positive anomalies over the central-eastern Pacific depicted an eastward shift and weakening of the PWC. This eastward shift of the PWC induced large-scale subsidence over the western Pacific, which in turn generated the low-level anticyclone over the South China Sea (10–30°N, 110–130°E; Figure 2b).

Under La Niña–like conditions, Ψ increased by ~8 units over 120°E–150°W, reflecting strengthened PWC ascent west of the Date Line, while modest weakening (−1 to −5 units) occurred over 150°W–90°W (Figure 6c). This pattern suggests a westward intensification of the Walker Circulation. This process enhanced deep convection over the western Pacific warm pool, which acts as a primary diabatic heating source. The associated heating anomaly induced a poleward-propagating Rossby wave train, leading to the development and maintenance of a low-level cyclonic anomaly over the East China Sea (20–40°N, 110–140°E; Figure 2c).

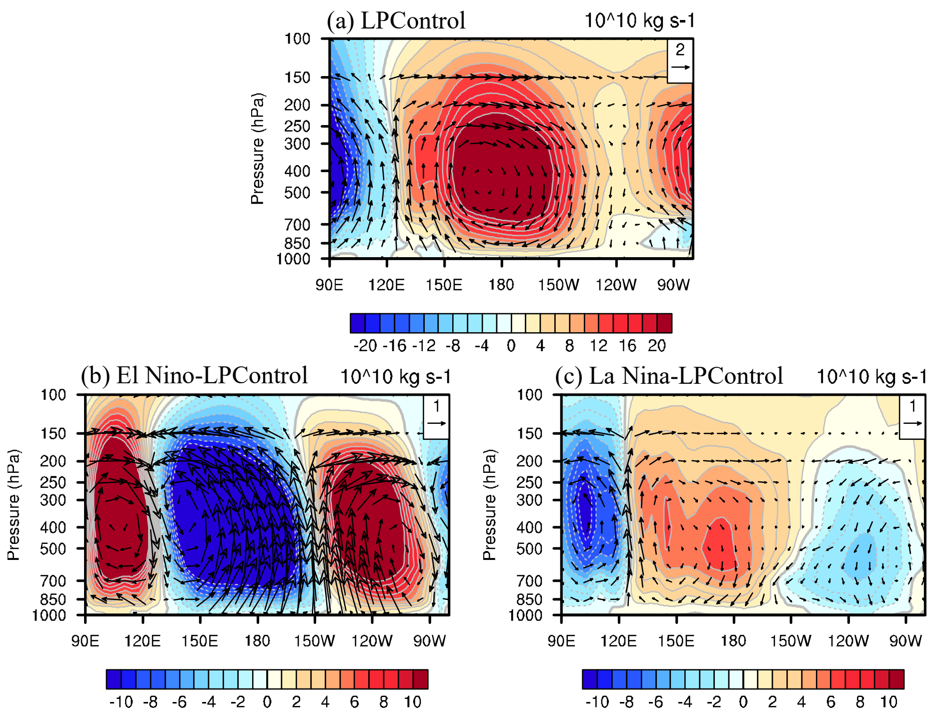

Figure 6. Boreal summer Walker circulation and its changes. (a) Boreal summer Walker circulation for the late Pliocene control experiment; (b) Summer changes in the tropical Pacific Walker circulation between the El Niño experiment and the late Pliocene control experiment; and (c) Summer changes in the tropical Pacific Walker circulation between the La Niña experiment and the late Pliocene control experiment. Summer spans June–August (JJA). Shading and contours are for zonal mass streamfunction (units: 10^{10} kg s^{-1}) along the equatorial Pacific (5°S–5°N). Vectors are the composite of pressure velocity ($\omega \times -50$; units: Pa s^{-1}) and zonal divergent wind (units: m s^{-1}).

4.4 Synthesis of mechanisms

In summary, the precipitation changes over East Asia under Pliocene-like warmth arise from the combined effects of thermodynamic and dynamic processes. The warmer background, driven by elevated atmospheric CO_2 concentrations, increases the moisture-holding capacity of the atmosphere via the Clausius–Clapeyron relationship. This thermodynamic effect ensures that any circulation anomaly—whether an anticyclone or a cyclone—advects moisture-laden air masses, contributing to the overall wetting across East Asia in both ENSO phases.

The spatial distribution of the enhanced rainfall, however, is dictated by ENSO-specific dynamic adjustments (Figure 7). For El Niño, an eastward-shifted Walker Circulation triggers anomalous subsidence over the western Pacific, exciting a low-level anticyclone over the South China Sea and a southward-shifted westerly jet via a Rossby wave train. This configuration channels moisture from the South China Sea toward southern China, where enhanced baroclinicity along the northern flank of the WPSH facilitates ascent. For La Niña, a westward-intensified Walker Circulation generates a low-level cyclone over the East China Sea and a mid-level coastal anticyclone over northeast Asia that splits the westerly jet. This pattern spreads moisture convergence across central-eastern China, producing widespread precipitation.

Thus, while the thermodynamic background guarantees the overall increase in precipitation, the specific circulation patterns induced by the ENSO phase determine the region where the heaviest rainfall occurs.

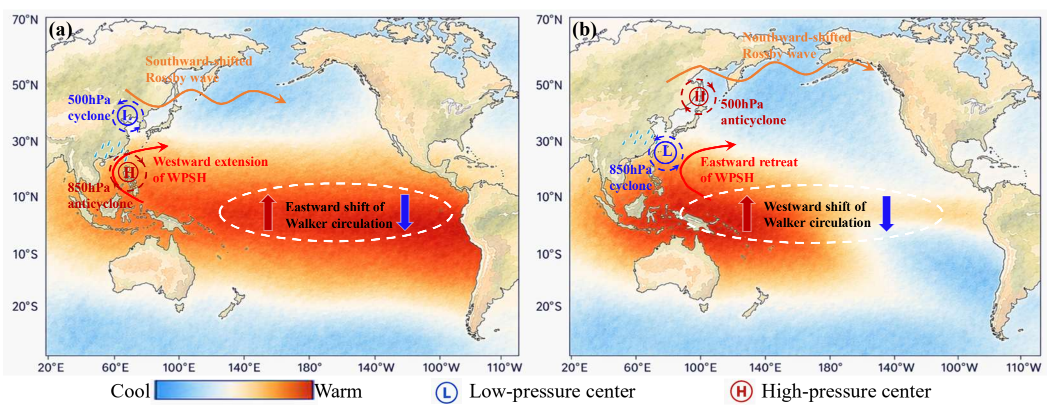

Figure 7. Schematic diagram summarizing the mechanisms by which El Niño (a) and La Niña (b) modulate the East Asian summer monsoon precipitation under Pliocene-like warmth.

5 Discussion

Several geological records and modeling studies indicate a weakened east–west sea surface temperature (SST) gradient in the tropical Pacific during the late Pliocene warm period, supporting the hypothesis of persistent El Niño–like conditions (Fedorov and Philander, 2001; Fedorov et al., 2006; Ravelo et al., 2004; Wara et al., 2005;

Winnick et al., 2013). However, other studies argued that late Pliocene east–west SST gradients were comparable to present-day values, refuting the notion of a permanent El Niño state (Bonham et al., 2009; Haywood et al., 2007; Pontes et al., 2022; Zhang et al., 2012; Zhang et al., 2013). Some reconstructions even suggested enhanced east–west SST gradients, analogous to La Niña–like conditions (Rickaby and Halloran, 2005; Watanabe et al., 2011).

Numerous geological records have demonstrated strengthened summer monsoon precipitation in East Asia during the Pliocene (Ding et al., 1999, 2001; Yang et al., 2018), and a systematic compilation of geological proxy records from across China also indicated widespread wet conditions over most of East Asia during the mid-Pliocene warm period (Huang et al., 2021), which is apparently analogous to the modern summer monsoon enhancement during La Niña phases (Chen et al., 2019; Gao et al., 2014). However, our results demonstrate that against a warmer climate background, both El Niño– and La Niña–like conditions lead to increased monsoon rainfall. Therefore, it is oversimplified to attribute Pliocene wetter conditions to a La Niña–like state based on modern analogs, as it ignores fundamental differences in Pliocene boundary conditions.

The global average temperature anomaly for January–November 2025 reached +1.48 °C relative to 1850–1900 (data from the Copernicus Climate Change Service), approaching the sustained +2–3 °C warmth characteristic of the LPWP. A recent study indicates that ongoing global warming has weakened the influence of ENSO on the EASM since the 2000s (Yu et al., 2025), which strongly supports our results. In contrast, another study found a strengthened trans-seasonal ENSO impact under future warming (Wang et al., 2025), suggesting that the response may depend on the warming stage or background state. This apparent discrepancy likely arises from the different timescales: Wang et al. (2025) focused on seasonal predictability, while our experiments examine mean-state responses under permanent ENSO conditions. It should be noted that our experiments are idealized permanent states, examining transient ENSO events against a warm background would help bridge the gap between our idealized permanent states and realistic climate variability. Future work should employ higher-resolution models, and more constrained boundary conditions to further quantify these dynamics and their regional manifestations.

6 Conclusions

Against the warm background conditions of the Pliocene, our simulation results demonstrate how El Niño/La Niña influences East Asian summer rainfall. Contrary to the opposite spatial pattern of modern precipitation over East Asia caused by the two ENSO phases (El Niño and La Niña), both El Niño– and La Niña–like states produced a net increase in summer precipitation over continental East Asia. This consistent wetting response was primarily enabled by the elevated moisture-holding capacity of the warmer atmosphere, which provided abundant moisture supply and enhanced the efficiency of rainfall generation, regardless of the ENSO phase.

The increased monsoon precipitation, however, was dictated by distinct dynamical processes. During El Niño, a low-level anticyclone over the South China Sea and a southward-displaced westerly jet—guided by a Rossby wave train with a trough near 150°E—focused the moisture transport and generated an upward motion, leading to increased rainfall over South China. During La Niña, a low-level cyclone over the East China Sea and a coastal anticyclone pumped moisture inland, while the westerly jet steered convergence to central-eastern China, resulting in a broad precipitation increase there. Our findings suggest that both ENSO extremes could exacerbate flood risks in populous East Asia under sustained warming, which highlights the hydroclimatic challenges of a future warmer world.

Acknowledgements

This study was supported by the Strategy Priority Research Program (Category B) of Chinese Academy of Sciences (XDB0710000), and the National Natural Science Foundation of China (42572023, 42503058).

Conflict of Interest

The authors declare no conflicts of interest relevant to this study.

Data Availability Statement

The data presented in the figures are available from Science Data Bank (https://www.scidb.cn/en/s/fIRjai).

References

Back, L., Russ, K., Liu, Z., Inoue, K., Zhang, J., & Otto-Bliesner, B. (2013). Global hydrological cycle response to rapid and slow global warming. *Journal of Climate*, 26, 8781–8786.

Bonham, S. G., Haywood, A. M., Lunt, D. J., Collins, M., & Salzmann, U. (2009). El Niño–southern oscillation, Pliocene climate and equifinality. *Philosophical Transactions of the Royal Society A: Mathematical, Physical and Engineering Sciences*, 367, 127–156.

Bragg, F. J., Lunt, D. J., & Haywood, A. M. (2012). Mid-Pliocene climate modelled using the UK Hadley Centre Model: PlioMIP Experiments 1 and 2. *Geoscientific Model Development*, 5, 1109–1125. https://doi.org/10.5194/gmd-5-1109-2012

Burke, K. D., Williams, J. W., Chandler, M. A., Haywood, A. M., Lunt, D. J., & Otto-Bliesner, B. L. (2018). Pliocene and Eocene provide best analogs for near-future climates. *Proceedings of the National Academy of Sciences*, 115(52), 13288–13293.

Cai, W., Santoso, A., Collins, M., Dewitte, B., Karamperidou, C., Kug, J.-S., et al. (2021). Changing El Niño–Southern Oscillation in a warming climate. *Nature Review Earth & Environment*, 2, 628–644. https://doi.org/10.1038/s43017-021-00199-z

Cane, M. A., (2005). The evolution of El Niño, past and future. *Earth and Planetary Science Letters*, 230, 227–240.

Chen, L., Gu, W. & Li, W. (2019). Why Is the East Asian Summer Monsoon Extremely Strong in 2018?—Collaborative Effects of SST and Snow Cover Anomalies. *Journal of Meteorological Research*, 33, 593–608. https://doi.org/10.1007/s13351-019-8200-4

Chen, L. X., Zhu, Q. G., Luo, H. B., He, J., Dong, M., & Feng, Z. (1991). East Asian Monsoon (in Chinese), China Meteorological Press, Beijing, pp. 200–240.

Ding, Y. H. (2004). Seasonal march of the East-Asian summer monsoon. In: Chang C P, ed. East Asian Monsoon. Singapore: World Scientific Publishing Co. Pte. Ltd. 3–53.

Ding, Z. L., Xiong, S. F., Sun, J. M., Yang, S. L., Gu, Z. Y., & Liu, T. S. (1999). Pedostratigraphy and paleomagnetism of a∼ 7.0 Ma eolian loess–red clay sequence at Lingtai, Loess Plateau, north-central China and the implications for paleomonsoon evolution. *Palaeogeography, Palaeoclimatology, Palaeoecology*, 152(1–2), 49–66.

Ding, Z. L., Yang, S. L., Sun, J. M., & Liu, T. S. (2001). Iron geochemistry of loess and red clay deposits in the Chinese Loess Plateau and implications for long-term Asian monsoon evolution in the last 7.0 Ma. *Earth and Planetary Science Letters*, 185(1–2), 99–109.

Dowsett, H., Dolan, A., Rowley, D., Moucha, R., Forte, A. M., Mitrovica, J. X., et al. (2016). The PRISM4 (mid-Piacenzian) paleoenvironmental reconstruction. *Climate of the Past*, 12(7), 1519–1538.

Edwards, J. M., & Slingo, A. (1996) Studies with a flexible new radiation code. I: Choosing a configuration for a large-scale model. *Quarterly Journal of the Royal Meteorological Society*, 122(531), 689–719. https://doi.org/10.1002/qj.49712253107

Fedorov, A. V., Dekens, P. S., McCarthy, M., Ravelo, A. C., DeMenocal, P. B., Barreiro, M., et al. (2006). The Pliocene paradox (mechanisms for a permanent El Niño). *Science*, 312, 1485–1489.

Fedorov, A. V., & Philander, S. G. (2001). A stability analysis of tropical ocean–atmosphere interactions: bridging measurements and theory for El Niño. *Journal of Climate*, 14, 3086–3101.

Galeotti, S., von der Heydt, A., Huber, M., Bice, D., Dijkstra, H., Jilbert, T., et al. (2010). Evidence for active El Niño Southern Oscillation variability in the late Miocene greenhouse climate. *Geology*, 38, 419–422. https://doi.org/10.1130/G30629.1

Gao, H., Jiang, W., & Li, W. (2014). Changed relationships between the East Asian summer monsoon circulations and the summer rainfall in eastern China. *Journal of Meteorological Research*, 28, 1075–1084. https://doi.org/10.1007/s13351-014-4327-5

Gordon, C., Cooper, C., Senior, C. A., Banks, H., Gregory, J. M., Johns, T. C., et al. (2000). The simulation of SST, sea ice extents and ocean heat transports in a version of the Hadley Centre coupled model without flux adjustments. *Climate Dynamics*, 16(2), 147–168. https://doi.org/10.1007/s003820050010

Haywood, A. M., Dolan, A. M., Pickering, S. J., Dowsett, H. J., Mcclymont, E. L., Prescott, C. L., et al. (2013). On the identification of a Pliocene time slice for data–model comparison. *Philosophical Transactions of the Royal Society A*, 371, 20120515.

Haywood, A. M., Dowsett, H. J., Dolan, A. M., Rowley, D., Abe-Ouchi, A., Otto-Bliesner, B., et al. (2016). The Pliocene Model Intercomparison Project (PlioMIP) Phase 2: scientific objectives and experimental design. *Climate of the Past*, 12, 663–675. https://doi.org/10.5194/cp-12-663-2016

Haywood, A. M., Dowsett, H. J., Otto-Bleisner, B., Chandler, M. A., Dolan, A. M., Hill, D. J., et al. (2010). Pliocene Model Intercomparison Project (PlioMIP): experimental design and boundary conditions (Experiment 1). *Geoscientific Model Development*, 3, 227–242.

Haywood, A. M., Dowsett, H. J., Robinson, M. M., Stoll, D. K., Dolan, A. M., Lunt, D. J., et al. (2011). Pliocene Model Intercomparison Project (PlioMIP): experimental design and boundary conditions (Experiment 2). *Geoscientific Model Development*, 4, 571–577. https://doi.org/10.5194/gmd-4-571-2011

Haywood, A. M., Valdes, P. J., & Peck, V. L. (2007). A permanent El Niño–like state during the Pliocene? *Paleoceanography*, 22, PA1213.

Hu, K., Xie, S. P., & Huang, G. (2017). Orographically anchored El Niño effect on summer rainfall in central China. *Journal of Climate*, 30, 10037–10045.

Huang, R., & Wu, Y. (1989). The influence of ENSO on the summer climate change in China and its mechanism. *Advances in Atmospheric Sciences*, 6(1), 21–32.

Huang, X., Jiang, D., Dong, X., Yang, S., Su, B., Li, X., et al. (2019). Northwestward migration of the northern edge of the East Asian summer monsoon during the mid-Pliocene warm period: Simulations and reconstructions. *Journal of Geophysical Research: Atmospheres*, 124(3), 1392–1404. https://doi.org/10.1029/2018JD028995

Huang, X., Yang, S., Haywood, A., Jiang, D., Wang, Y., Sun, M., et al. (2021). Warming-induced northwestward migration of the Asian summer monsoon in the geological past: Evidence from climate simulations and geological reconstructions. *Journal of Geophysical Research: Atmospheres*, 126(18), e2021JD035190. https://doi.org/10.1029/2021JD035190

Huang, X., Yang, S., Haywood, A., Tindall, J., Sun, M., Yang, X., et al. (2026). Dataset for weakened El Niño/La Niña influence on the East Asian summer monsoon under Pliocene warmth: Insights from model sensitivity experiments [Dataset]. Science Data Bank. https://doi.org/10.57760/sciencedb.34744

Huang, Y., Wang, H., Fan, K., & Gao, Y. (2015). The western Pacific subtropical high after the 1970s: westward or eastward shift? *Climate Dynamics*, 44(7–8), 2035–2047. https://doi.org/10.1007/s00382-014-2194-5

Hunter, S. J., Haywood, A. M., Dolan, A. M., & Tindall, J. C. (2019). The HadCM3 contribution to PlioMIP phase 2. *Climate of the Past*, 15(5), 1691–1713. https://doi.org/10.5194/cp-15-1691-2019

Intergovernmental Panel on Climate Change (2013). *Climate Change 2013: The Physical Science Basis*. Contribution of Working Group I to the Fifth Assessment Report of the Intergovernmental Panel on Climate Change, Cambridge, UK, New York: Cambridge University Press.

Ivany, L. C., Brey, T., Huber, M., Buick, D. P., & Schöne, B. R. (2011). El Niño in the Eocene greenhouse recorded by fossil bivalves and wood from Antarctica. *Geophysical Research Letters*, 38, L16709. https://doi.org/10.1029/2011GL048635

Jiang, D. B., Wang, H., Helge, D., & Lang, X. (2004). Instability of the East Asian summer monsoon-ENSO relationship in a coupled global atmosphere-ocean GCM (in Chinese). *Chinese Journal of Geophysics*, 47(6), 976–981,

Levitus, S., Antonov, J. I., Boyer, T. P., & Stephens, C. (2000). Warming of the world ocean. *Science*, 287, 2225–2229.

Li, M., Jia, W., Yang, Y., Cheng, H., Zhao, J., He, S., et al. (2026). Spatial patterns of Asian summer monsoon precipitation in the Chinese monsoon region since the LGM. *npj Climate and Atmospheric Science*, 9, 67. https://doi.org/10.1038/s41612-026-01345-4

Li, X., Hu, S., Hu, Y., Cai, W., Jin, Y., Lu, Z., et al. (2024). Persistently active El Niño–Southern Oscillation since the Mesozoic. *Proceedings of the National Academy of Sciences*, 121(45), e2404758121.

Liu, J., Wang, B., & Yang, J. (2008). Forced and internal modes of variability of the East Asian summer monsoon. *Climate of the Past*, 4(4), 225–233. https://doi.org/10.5194/cp-4-225-2008

Liu, X. D. (1999). Influences of Qinghai-Xizang (Tibet) plateau uplift on the atmospheric circulation global climate and environment changes. *Plateau Meteorology*, 18, 321–332

Liu, Z. Y., Kutzbach, J., & Wu, L. X. (2000). Modeling climate shift of El Niño variability in the Holocene. *Geophysical Research Letters*, 27, 2265–2268.

Long, Z. X., & Li, C. Y. (2001). Numerical simulation of lag influence of ENSO on East-Asian monsoon. *Journal of Meteorological Research*, 15, 59–70.

Manucharyan, G. E., & Fedorov, A. V. (2014). Robust ENSO across a wide range of climates. *Journal of Climate*, 27(15), 5836–5850.

McClymont, E. L., Ford, H. L., Ho, S. L., Tindall, J. C., Haywood, A. M., Alonso-Garcia, M., et al. (2020). Lessons from a high CO_2 world: an ocean view from ~3 million years ago. *Climate of the Past*, 16, 1599–1615.

Pontes, G. M., Taschetto, A. S., Sen Gupta, A., Santoso, A., Wainer, I., Haywood, A. M., et al. (2022). Mid-Pliocene El Niño/Southern Oscillation suppressed by Pacific intertropical convergence zone shift. *Nature Geoscience*, 15(9), 726–734.

Pope, V. D., Gallani, M. L., Rowntree, P. R., & Stratton, R. A. (2000). The impact of new physical parametrizations in the Hadley Centre climate model: HadAM3. *Climate Dynamics*, 16(2–3), 123–146.

Ravelo, A. C., Andreasen, D. H., Lyle, M., Lyle, A. O., & Wara, M. W. (2004). Regional climate shifts caused by gradual global cooling in the Pliocene epoch. *Nature*, 429, 263–267.

Rickaby, R. E. M., & Halloran, P. (2005). Cool La Niña during the warmth of the Pliocene? *Science*, 307, 1948–1952.

Song, F., & Zhou, T. (2015). The crucial role of internal variability in modulating the decadal variation of the East Asian summer monsoon–ENSO relationship during the twentieth century. *Journal of Climate*, 28, 7093–7107.

Sun, L., Yang, X. Q., Tao, L., Fang, J., & Sun, X. (2021). Changing impact of ENSO events on the following summer rainfall in eastern China since the 1950s. *Journal of Climate*, 34(20), 8105–8123.

Sun, X. G., Greatbatch, R. J., Park, W., & Latif, M. (2010). Two major modes of variability of the East Asian summer monsoon. *Quarterly Journal of the Royal Meteorological Society*, 136, 829–841. https://doi.org/10.1002/qj.635

Tian, S., Dai, G., Yin, Q., Meng, X., Zhang, Z., Zhu, Z., & Xiao, G. (2022). Spatial differences in East Asian climate transition at ~260 ka and their links to ENSO. *Quaternary Science Reviews*, 296, 107805.

Trenberth, K. E., Fasullo, J., & Smith, L. (2005). Trends and variability in column-integrated atmospheric water vapour. *Climate Dynamics*, 24, 741–758.

Trenberth, K. E., Caron, J. M., Stepaniak, D. P., & Worley, S. (2002). Evolution of El Niño–Southern Oscillation and global atmospheric surface temperatures. *Journal of Geophysical Research: Atmospheres*, 107, 1–17.

Valdes, P. J., Armstrong, E., Badger, M. P. S., Bradshaw, C. D., Bragg, F., Crucifix, M., et al. (2017). The BRIDGE HadCM3 family of climate models: HadCM3@Bristol v1.0, *Geoscientific Model Development*, 10, 3715–3743. https://doi.org/10.5194/gmd-10-3715-2017

Wang, B., Wu, R., & Fu, X. (2000). Pacific–East Asian teleconnection: how does ENSO affect East Asian climate? *Journal of climate*, 13(9), 1517–1536.

Wang, H. J., & Fan, K. (2013). Recent Changes in the East Asian Monsoon (in Chinese). *Chinese Journal of the Atmospheric Sciences*, 37, 313–318.

Wara, M. W., Ravelo, A. C., & Delaney, M. L. (2005). Permanent El Niño-like conditions during the Pliocene warm period. *Science*, 309, 758–761.

Watanabe, T., Suzuki, A., Minobe, S., Kawashima, T., Kameo, K., Minoshima, K., et al. (2011). Permanent El Niño during the Pliocene warm period not supported by coral evidence. *Nature*, 471(7337), 209–211.

Webster, P. J., Magaña, V., Palmer, T. N., Shukla, J., Tomas, R. A., Yanai, M., & Yasunari, T. (1998). Monsoons: Processes, predictability, and the prospects for prediction. *Journal of Geophysical Research: Oceans*, 103, 14451–14510.

White, S. M., & Ravelo, A. C. (2020). Dampened El Niño in the early Pliocene warm period. *Geophysical Research Letters*, 47(4), e2019GL085504.

Winnick, M. J., Welker, J. M., & Chamberlain, C. P. (2013). Stable isotopic evidence of El Niño-like atmospheric circulation in the Pliocene Western United States. *Climate of the Past*, 9, 903–912.

Wu, Z., Schnieder, E. K., Hu, Z. Z., & Cao, L. (2001). The impact of global warming on ENSO variability in climate records. *Calverton: Center for Ocean-Land-Atmosphere Studies*, 110, 1–22.

Wycech, J. B., Gill, E., Rajagopalan, B., Marchitto, T. M. & Molnar, P. H. (2020). Multiproxy reduced-dimension reconstruction of Pliocene equatorial Pacific sea surface temperatures. *Paleoceanography and Paleoclimatology*, 35, e2019PA003685.

Xia, Y., Sun, X., Yan, Y., Feng, W., Huang, F., & Yang, X. (2017). Change of ENSO characteristics in response to global warming (in Chinese). *Chinese Science Bulletin*, 62(16), 1738–1751.

Xie, S. P., Kosaka, Y., Du, Y., Hu, K., Chowdary, J. S., & Huang, G. (2016). Indo-western Pacific Ocean capacitor and coherent climate anomalies in post-ENSO summer: A review. *Advances in Atmospheric Sciences*, 33(4), 411–432.

Yang, K., Cai, W., Huang, G., Hu, K., Ng, B., & Wang, G. (2022). Increased variability of the western Pacific subtropical high under greenhouse warming. *Proceedings of the National Academy of Sciences*, 119(23), e2120335119.

Yang, S., Ding, Z., Feng, S., Jiang, W., Huang, X., & Guo, L. (2018). A strengthened East Asian summer monsoon during Pliocene warmth: Evidence from 'red clay' sediments at Pianguan, northern China. *Journal of Asian Earth Sciences*, 155(15), 124–133.

Yu, B., & Zwiers, F. W. (2010). Changes in equatorial atmospheric zonal circulations in recent decades. *Geophysical Research Letters*, 37(5), L05701.

Yu, B., Zwiers, F. W., Boer, G. J., & Ting, M. F. (2012). Structure and variances of equatorial zonal circulation in a multimodel ensemble. *Climate Dynamics*, 39(9), 2403–2419.

Yu, T., Chen, W., Huang, P., Huang, G., & Yang, X. (2025). Weakened influence of ENSO on the East Asian summer monsoon since the early 2000s. *npj Climate and Atmospheric Science*, 8(1), 114.

Zhang, P., Xie, S. P., Kosaka, Y., Lutsko, N. J., Okumura, Y. M., & Miyamoto, A. (2024). Why East Asian monsoon anomalies are more robust in post El Niño than in post La Niña summers. *Nature Communications*, 15(1), 7401.

Zhang, R., Jiang, D., & Tian, Z. (2013). Permanent El Niño-like conditions during the middle Pliocene?—a coupled model results (in Chinese). *Quaternary Sciences*, 33(6), 1130–1137. https://doi.org/10.3969/j.issn.1001-7410.2013.06.09

Zhang, Z. S., Yan, Q., Su, J. Z., & Gao, Y. Q. (2012). Has the problem of a permanent El Niño been resolved for the mid-Pliocene? *Atmospheric and Oceanic Science Letters*, 5, 445–448.

Zhu, C. W., Chen, L. X., & Nobuo, Y. (1999). The interdecadal variation characteristics of Arctic sea ice cover-ENSO-east Asian monsoon and their interrelationship at quasi-four years time scale. *Advances in Atmospheric Sciences*, 16, 641–652.

Figure 1.

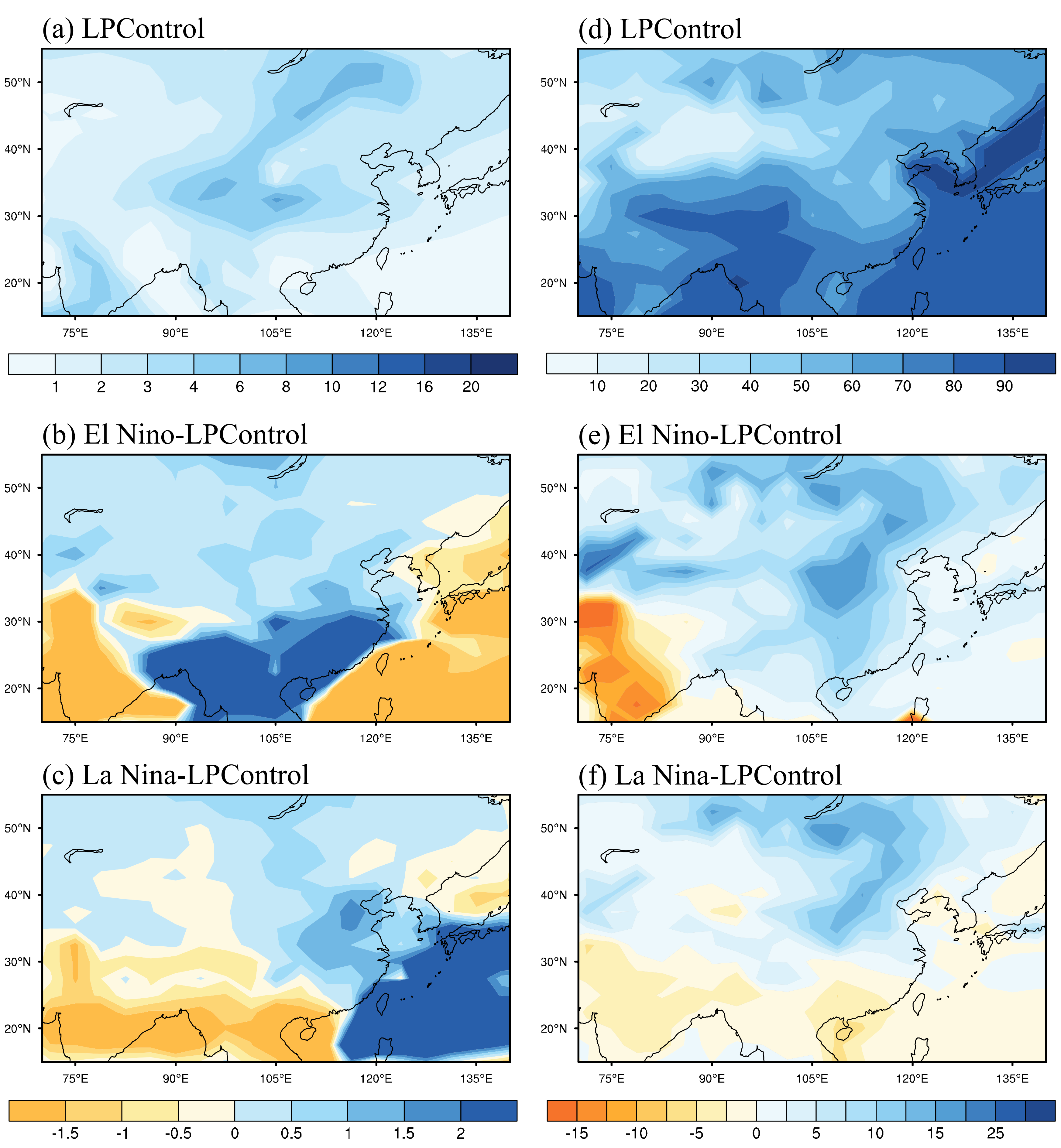
(a) LPControl
(b) El Nino-LPControl
(c) La Nina-LPControl
(d) LPControl
(e) El Nino-LPControl
(f) La Nina-LPControl
50°N
40°N
30°N
20°N
75°E
90°E
105°E
120°E
135°E
1 2 3 4 6 8 10 12 16 20
10 20 30 40 50 60 70 80 90
-1.5 -1 -0.5 0 0.5 1 1.5 2
-15 -10 -5 0 5 10 15 25

Figure 2.

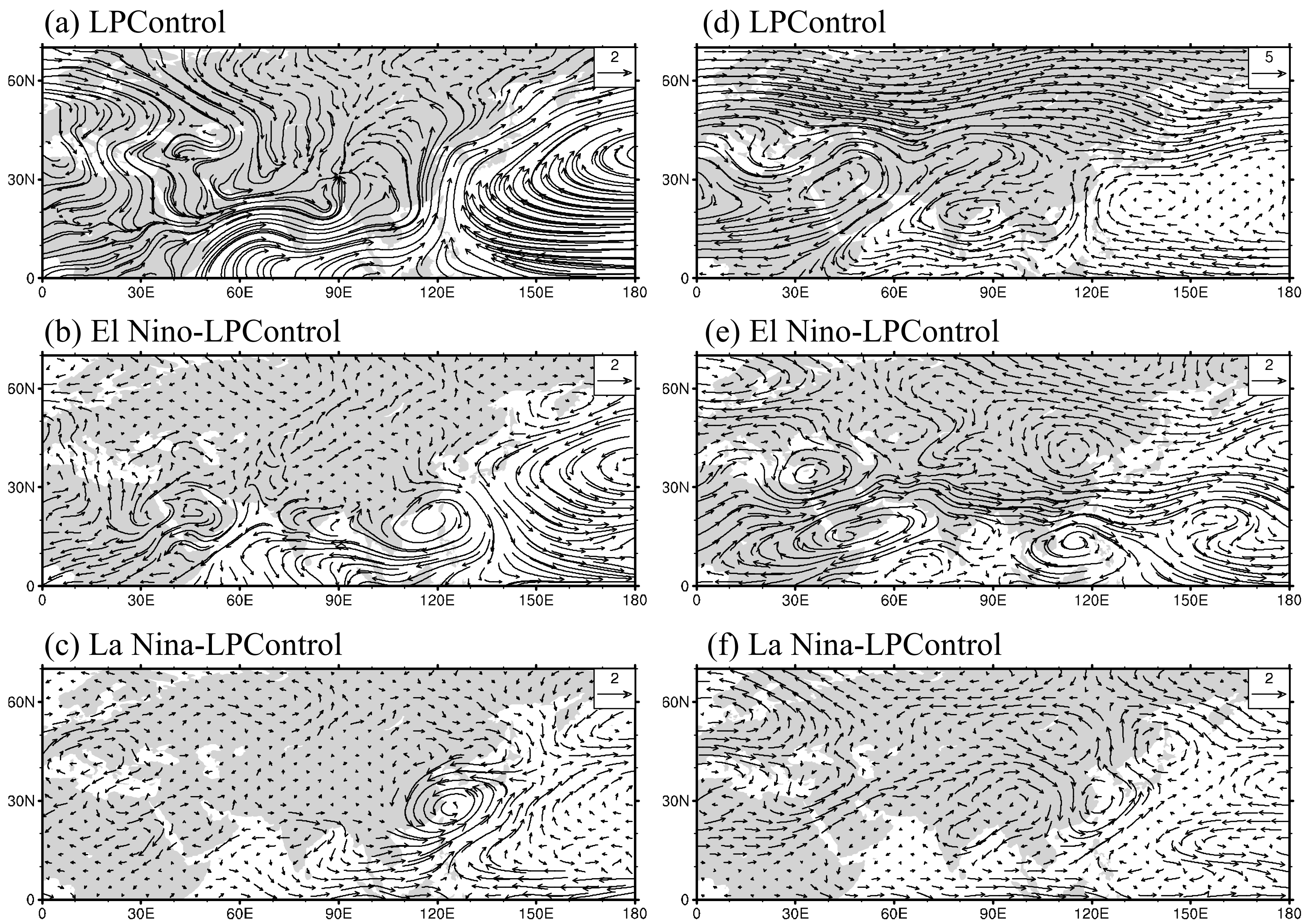
(a) LPControl
(b) El Nino-LPControl
(c) La Nina-LPControl
(d) LPControl
(e) El Nino-LPControl
(f) La Nina-LPControl
2
5
60N
30N
0
30E
60E
90E
120E
150E
180

Figure 3.

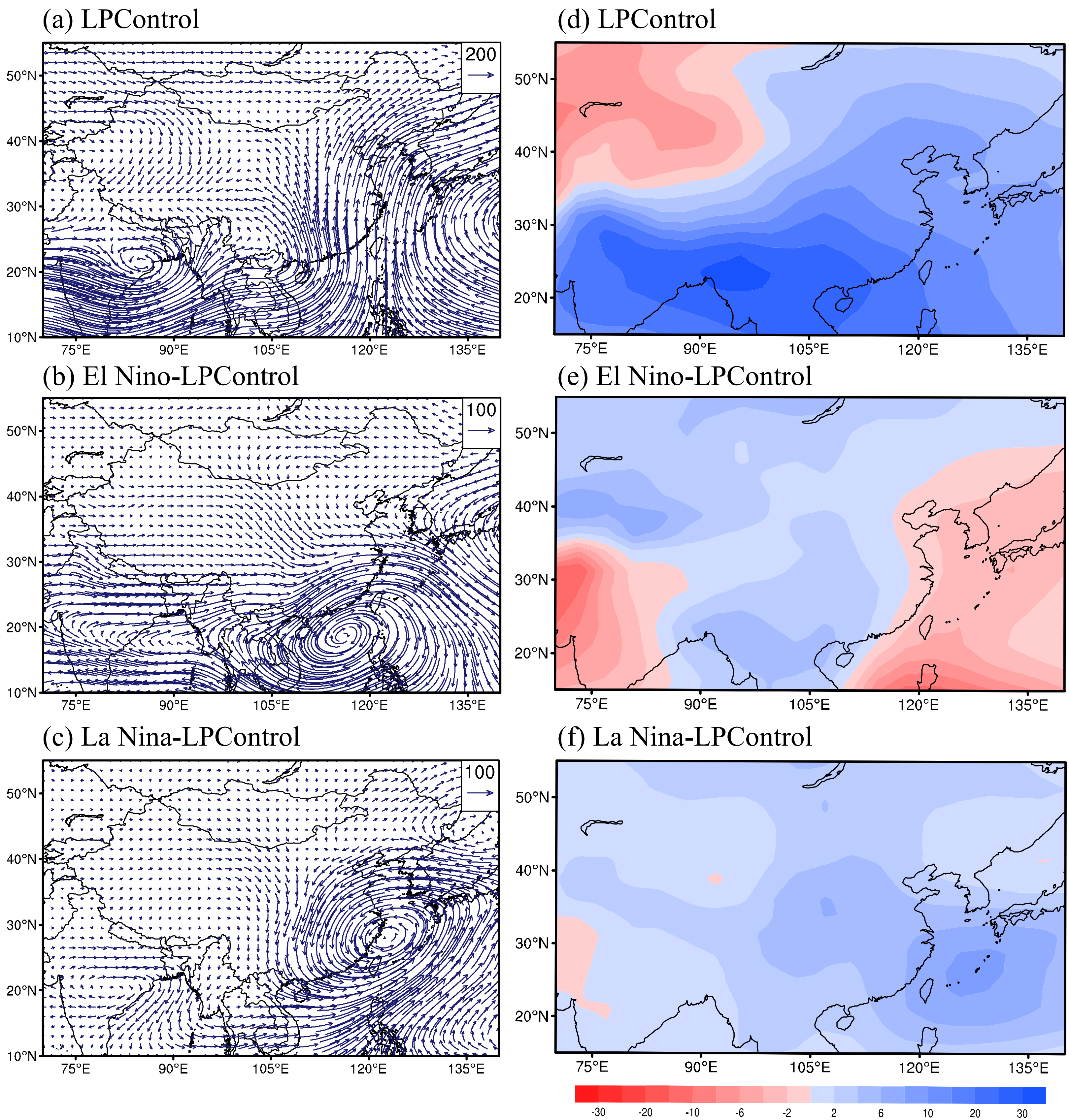

(a) LPControl
(b) El Nino-LPControl
(c) La Nina-LPControl
(d) LPControl
(e) El Nino-LPControl
(f) La Nina-LPControl
200
100
100
10°N
20°N
30°N
40°N
50°N
75°E
90°E
105°E
120°E
135°E
-30
-20
-10
-6
-2
2
6
10
20
30

Figure 4.

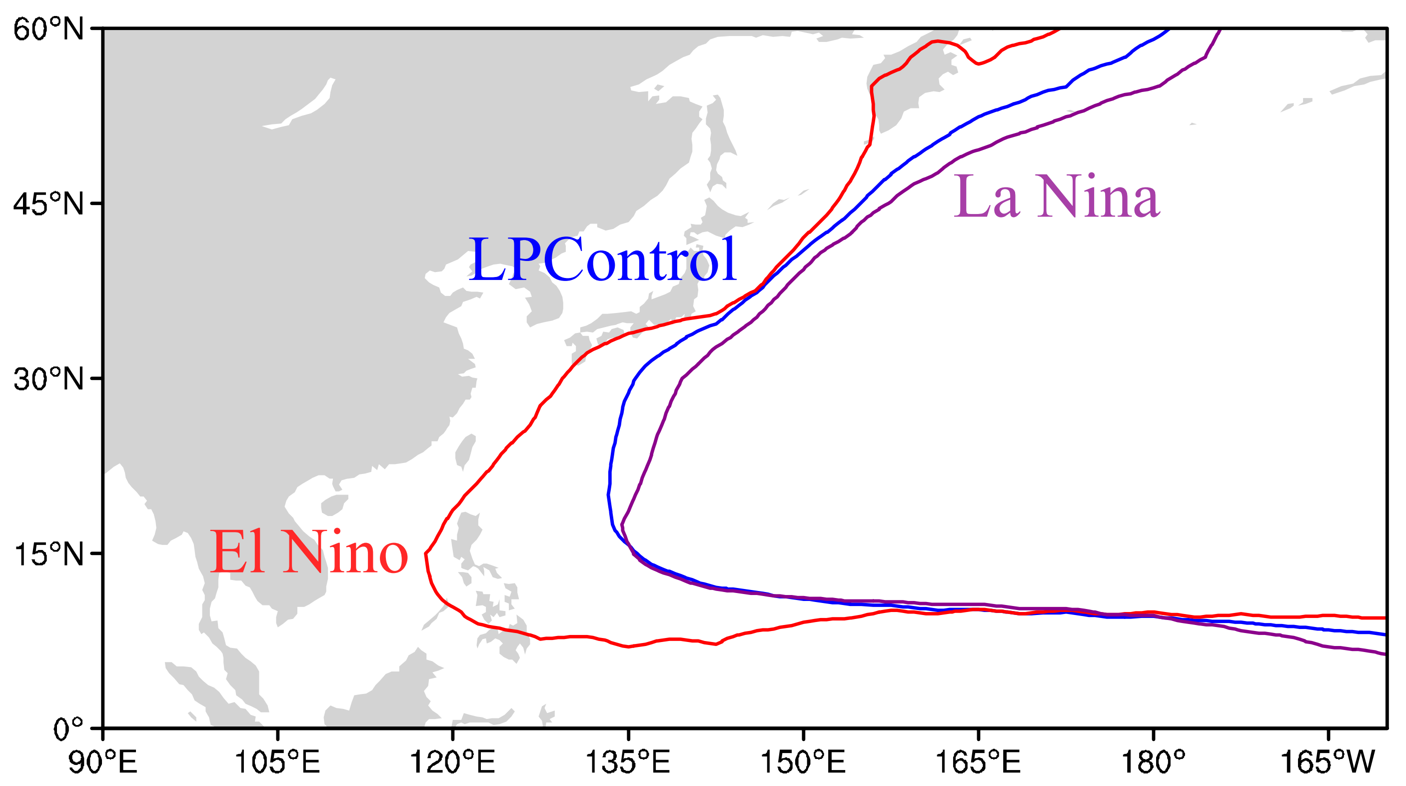

60°N
45°N
30°N
15°N
0°
90°E
105°E
120°E
135°E
150°E
165°E
180°
165°W
LPControl
La Nina
El Nino

Figure 5.

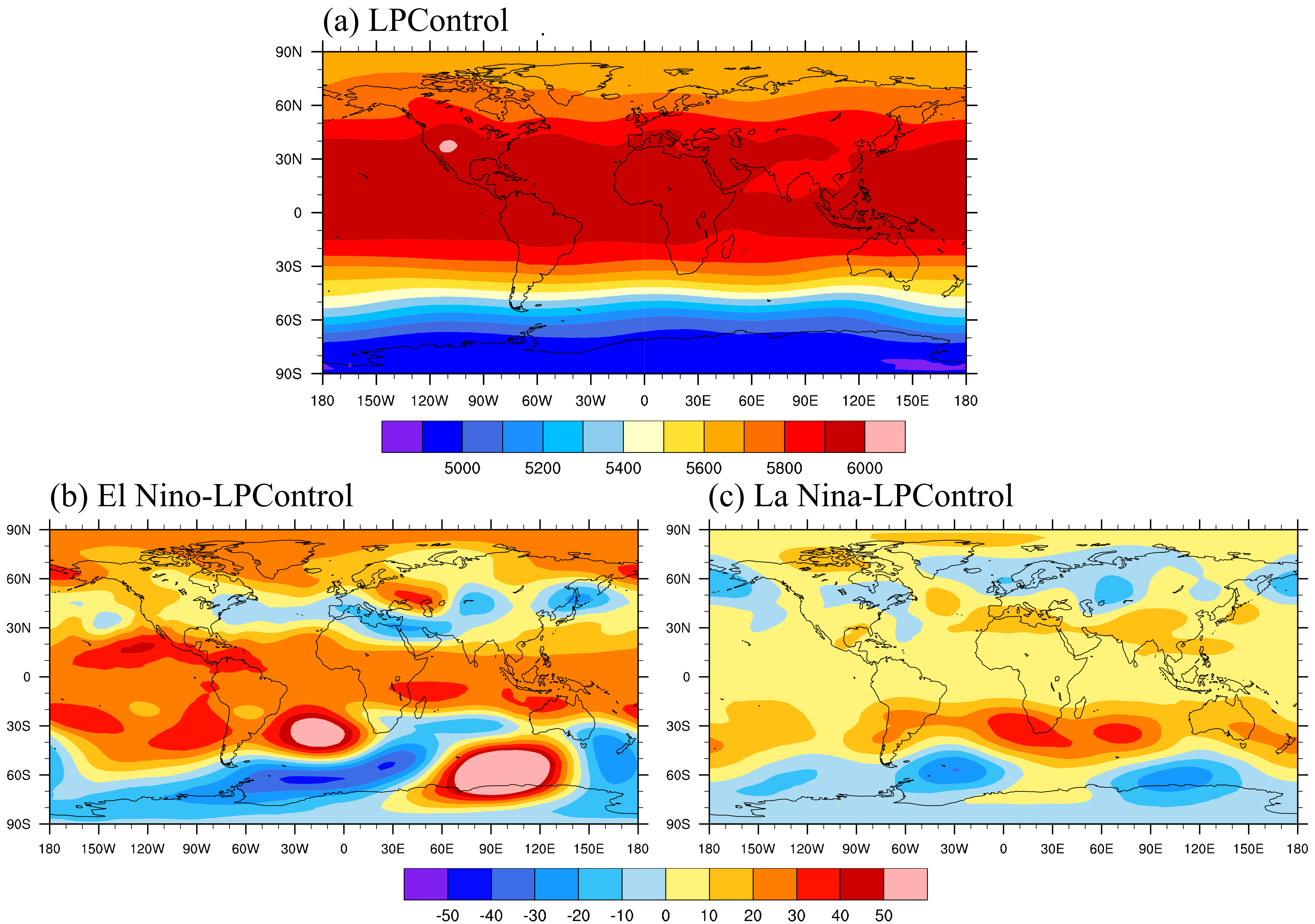

(a) LPControl
90N
60N
30N
0
30S
60S
90S
180
150W
120W
90W
60W
30W
0
30E
60E
90E
120E
150E
180
5000
5200
5400
5600
5800
6000
(b) El Nino-LPControl
(c) La Nina-LPControl
-50
-40
-30
-20
-10
0
10
20
30
40
50

Figure 6.

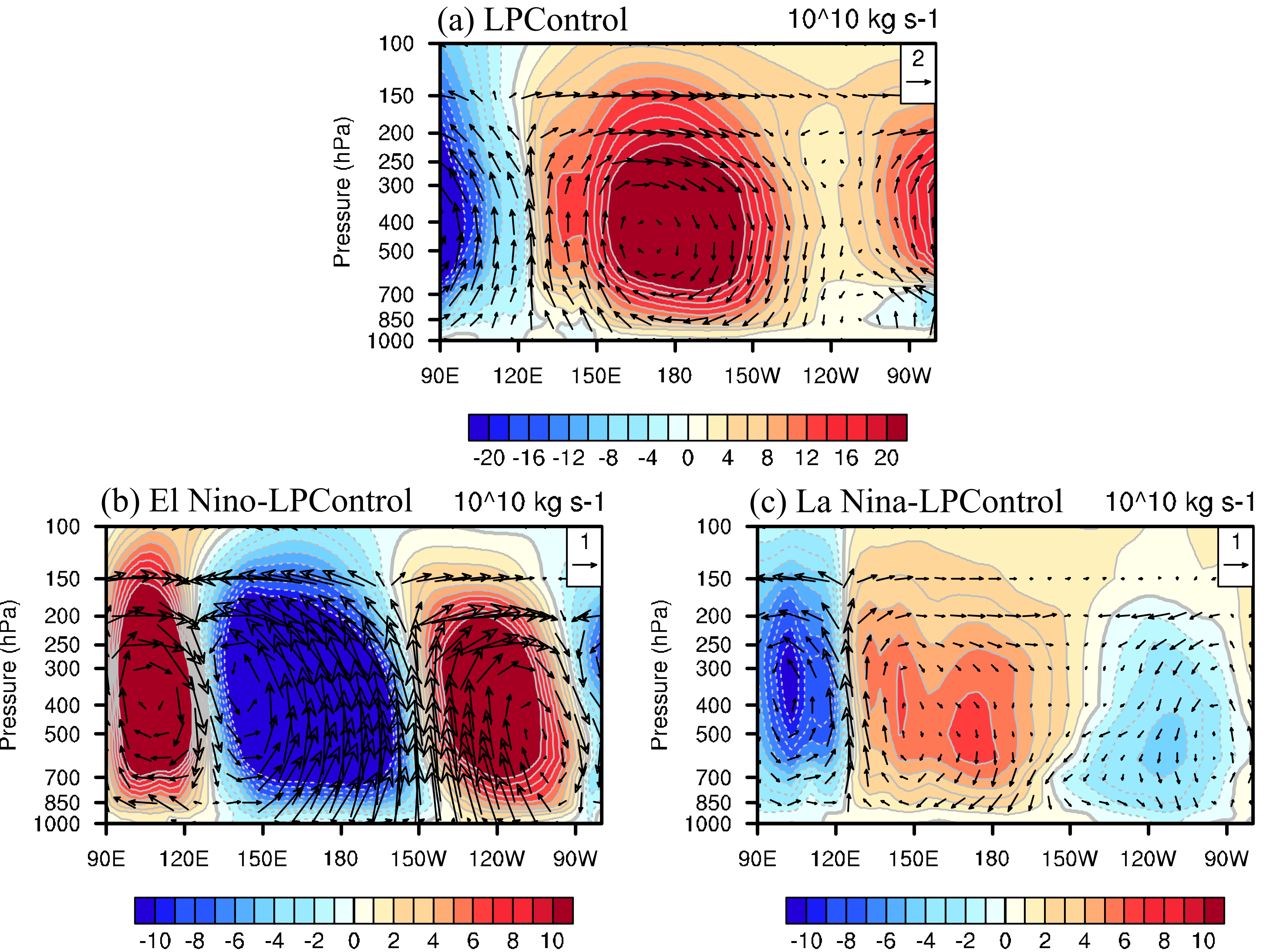

(a) LPControl
10^10 kg s-1
2
Pressure (hPa)
100
150
200
250
300
400
500
700
850
1000
90E
120E
150E
180
150W
120W
90W
-20 -16 -12 -8 -4 0 4 8 12 16 20
(b) El Nino-LPControl
10^10 kg s-1
1
Pressure (hPa)
-10 -8 -6 -4 -2 0 2 4 6 8 10
(c) La Nina-LPControl
10^10 kg s-1
1
Pressure (hPa)
-10 -8 -6 -4 -2 0 2 4 6 8 10

Figure 7.

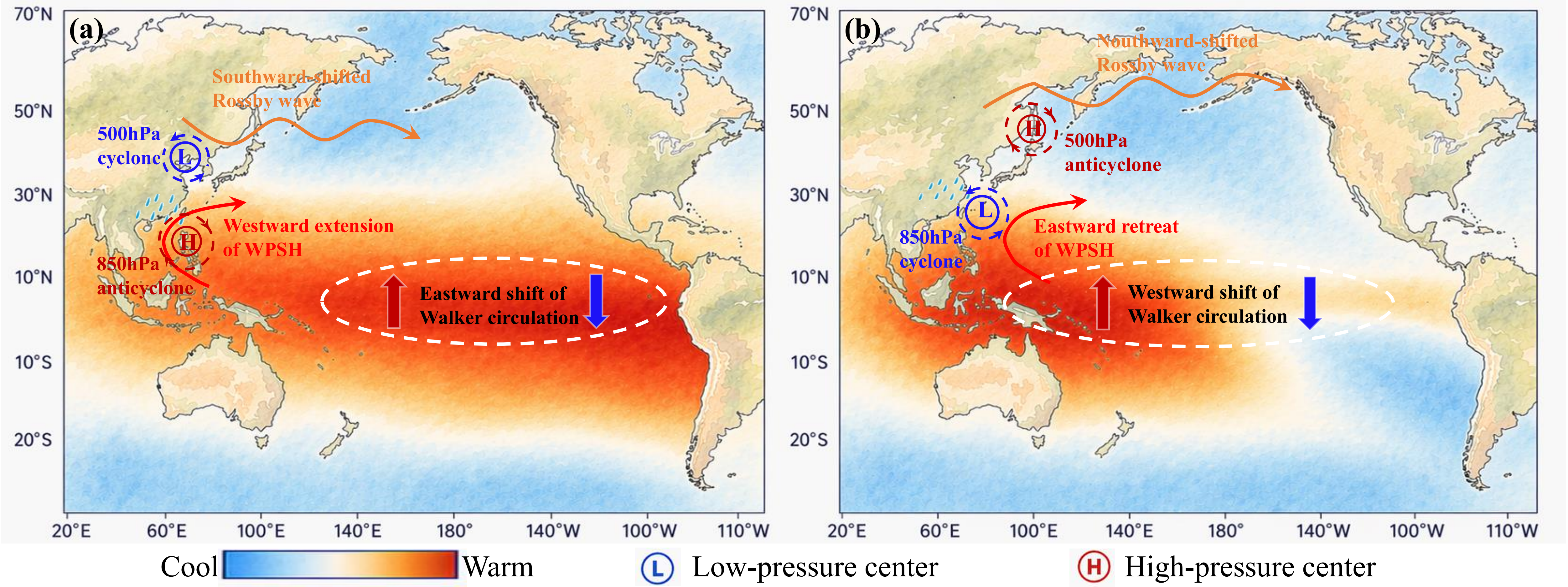
(a)
Southward-shifted
Rossby wave
500hPa
cyclone
Westward extension
of WPSH
850hPa
anticyclone
Eastward shift of
Walker circulation
(b)
Nouthward-shifted
Rossby wave
500hPa
anticyclone
850hPa
cyclone
Eastward retreat
of WPSH
Westward shift of
Walker circulation
70°N
50°N
30°N
10°N
10°S
20°S
20°E
60°E
100°E
140°E
180°
140°W
100°W
110°W
Cool
Warm
Low-pressure center
High-pressure center